

# Dalton Transactions

Accepted Manuscript

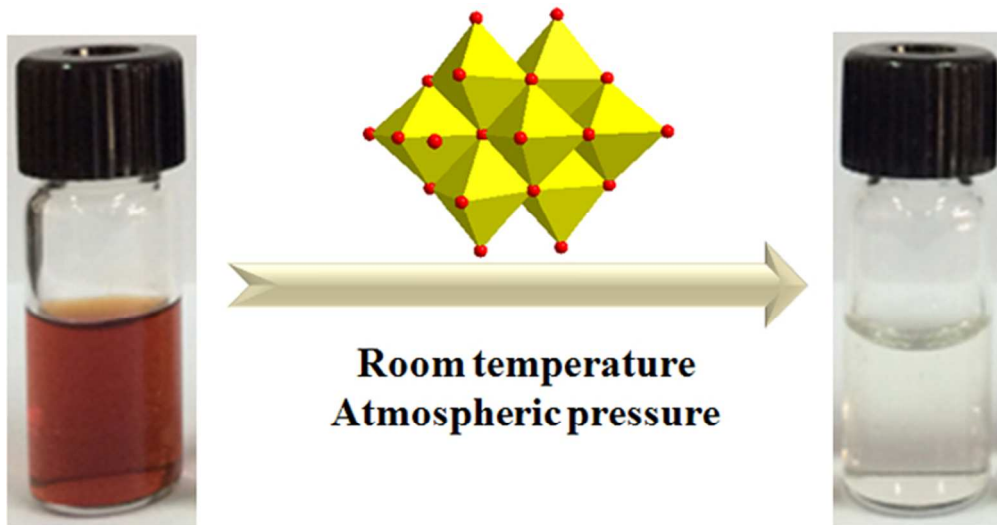


This is an *Accepted Manuscript*, which has been through the Royal Society of Chemistry peer review process and has been accepted for publication.

*Accepted Manuscripts* are published online shortly after acceptance, before technical editing, formatting and proof reading. Using this free service, authors can make their results available to the community, in citable form, before we publish the edited article. We will replace this *Accepted Manuscript* with the edited and formatted *Advance Article* as soon as it is available.

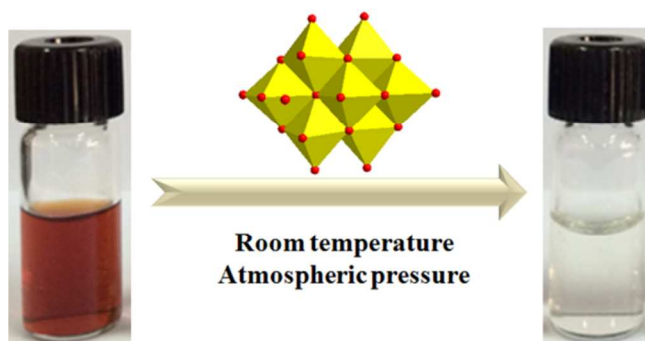
You can find more information about *Accepted Manuscripts* in the [Information for Authors](#).

Please note that technical editing may introduce minor changes to the text and/or graphics, which may alter content. The journal's standard [Terms & Conditions](#) and the [Ethical guidelines](#) still apply. In no event shall the Royal Society of Chemistry be held responsible for any errors or omissions in this *Accepted Manuscript* or any consequences arising from the use of any information it contains.



60x31mm (300 x 300 DPI)

Two new octamolybdate-based hybrid materials as catalysts for wet air oxidation of dyes under mild conditions



# Two novel octamolybdate nanoclusters as catalysts for dye degradation by air under room conditions

Mahnaz Najafi,<sup>a</sup> Alireza Abbasi,<sup>\*a</sup> Majid Masteri-Farahani<sup>b</sup> and Jan Janczak<sup>c</sup>

Dalton Transactions Accepted Manuscript

---

<sup>a</sup> School of Chemistry, College of Science, University of Tehran, Tehran, Iran. Fax: +98-21-66495291; [Tel: +98-21-61113644](tel:+98-21-61113644)  
E-mail: [aabbasi@khayam.ut.ac.ir](mailto:aabbasi@khayam.ut.ac.ir)

<sup>b</sup> Faculty of Chemistry, Kharazmi University, Tehran, Iran

<sup>c</sup> Institute of Low Temperature and Structure Research, Polish Academy of Sciences, PO Box 1410, 50-950 Wrocław, Poland.

## Abstract

Two novel inorganic-organic hybrid materials,  $(\text{NH}_4)_2\text{CuMo}_8\text{O}_{26}(\text{C}_{10}\text{H}_8\text{N}_2)_2$  (**1**) and  $\text{Mo}_8\text{O}_{26}(\text{C}_{10}\text{H}_{10}\text{N}_2)_2(\text{C}_{10}\text{H}_8\text{N}_2)_2(\text{H}_2\text{O})$  (**2**) have been synthesized based on  $\beta$ -octamolybdate cluster and 4,4'-bipyridine (4,4'-bpy) ligand under solvothermal conditions. Their structures have been determined by single-crystal X-ray diffraction analyses and characterized by means of FT-IR, atomic absorption spectroscopy, powder X-ray diffraction (PXRD) and thermogravimetric analysis (TGA). In addition, the microcrystals of **1** were used to synthesize its nanocrystals via ultrasound-assisted top-down method. The nanocrystals were characterized by scanning electron microscopy (SEM), PXRD and FT-IR analyses. The prepared hybrid materials have been proved to be active heterogeneous catalysts for catalytic wet air oxidation (CWAO) of some dyes under mild conditions. The leaching experiments showed that the catalysts had good stability under reaction conditions and could be easily recycled and reused after a simple treatment.

## Introduction

Wastewaters produced by textile industrial processes represent environmental danger owing to their toxicity and carcinogenic characteristic [1]. Azo dyes as the most important class of dyes have been widely used in various industries such as pharmaceutical, cosmetic, food, paper and clothing. The concern for the toxicity of these compounds has led to considerable efforts for their treatment [2].

Several methods such as electrochemical oxidation [3], photodegradation [4-6], enzymatic biodegradation [7], adsorption [8] and catalytic wet air oxidation (CWAO) [9] have been reported for color removal from wastewaters. Application of proper catalysts for CWAO is important from economical points of view and up to now many catalysts have been applied for the CWAO of pollutants including metal oxides [10-12] and polyoxometallates (POMs) [13-15].

POMs, as oxo-clusters of early transition metals in the highest oxidation state, have been shown to be promising environmental catalysts for the elimination of organic pollutants present in water [16-17]. However the high solubility of POMs in aqueous solutions and their low stability under catalytic conditions have limited their industrial applications due to the difficulty of separation and recovery of the catalyst after the oxidation process. Therefore considerable attention has been paid to the preparation of POM-based heterogeneous catalysts using solid supports or constructing self-supported inorganic-organic hybrid materials and coordination polymers [18-22].

Nano-structured coordination polymers have attracted interests owing to providing a novel opportunity to combine the variety of coordination polymers with the unique properties of nanomaterials. Ultrasound is a simple and economical technique that has been extensively utilized for the fabrication of nanostructured coordination polymers. Ultrasound radiation generates microscopic bubbles in the solvent during cavitation that involves the growth and implosive collapse of bubbles in a liquid. This phenomenon can provide energy to break down many precursors to nano-scale sizes or to induce chemical changes in them [23-27].

In the present work, two novel inorganic-organic hybrid compounds namely,  $(\text{NH}_4)_2\text{CuMo}_8\text{O}_{26}(\text{C}_{10}\text{H}_8\text{N}_2)_2$  (**1**) and  $\text{Mo}_8\text{O}_{26}(\text{C}_{10}\text{H}_{10}\text{N}_2)_2(\text{C}_5\text{H}_4\text{N})_2(\text{H}_2\text{O})_2$  (**2**) have been solvothermally synthesized based on octamolybdate clusters. Moreover, the light green crystals of **1** have been converted into nano-scale by sonochemical process. The prepared hybrid materials show an efficient catalytic activity for the degradation of some dye including Bismarck brown (BB), Azure II, Direct blue 71 (DB 71), Methyl violet (MV) and Methylene blue (MB) under mild conditions.

## Experimental

### Materials and characterization

All chemicals were purchased from commercial sources and used without further purification.

A multiwave ultrasonic generator (Sonicator 3200; Bandeline, KE 76, Germany), equipped with a converter/transducer and titanium oscillator (horn), 6 mm in diameter, operating at 50/60 Hz with a maximum power output of 200 W, was used for the ultrasonic irradiation. FT-IR spectra were acquired on Bruker Equinox 55 spectrometer equipped with a single reflection diamond ATR system over the range of 600-4000  $\text{cm}^{-1}$ . Powder X-ray diffraction (PXRD) patterns were measured on a Philips PW1800 diffractometer using  $\text{Cu K}\alpha$  radiation ( $\lambda = 1.5406 \text{ \AA}$ ). Thermogravimetric analysis (TGA) of the samples was carried out under argon atmosphere on a TGA Q 50 instrument with the heating rate of 20  $^\circ\text{C} \cdot \text{min}^{-1}$ . Scanning electron microscopy (SEM) was performed on a KYKY EM-3200. UV-Vis spectra were recorded on a Perkin Elmer Lambda 850 spectrophotometer. The metal content of the catalyst was determined using Contraa 700 atomic absorption spectrometer.

### Synthesis of $(\text{NH}_4)_2\text{CuMo}_8\text{O}_{26}(\text{C}_{10}\text{H}_8\text{N}_2)_2$ (**1**)

A mixture of  $(\text{NH}_4)_6\text{Mo}_7\text{O}_{24} \cdot 4\text{H}_2\text{O}$  (0.37 g),  $\text{Cu}(\text{NO}_3)_2 \cdot 3\text{H}_2\text{O}$  (0.048 g), 4,4'-bpy (0.14 g),  $\text{C}_2\text{H}_2\text{O}_4$  (0.001 g),  $\text{H}_2\text{O}$  (8 ml) and ethanol (2 ml) was stirred for 30 min in air. The suspension was transferred to a 23 ml Teflon-lined stainless-steel autoclave and heated at 160  $^\circ\text{C}$  for 5 days. After slow cooling to room temperature, the product was filtered, washed with distilled water and dried in air to yield light green crystals of **1**.

In order to synthesize **1** in nano-scale, the crystals of the prepared coordination polymer (0.1 g) were added to water (10 ml) and then the mixture was exposed to ultrasonic irradiation at 50 % of power for 15 min.

The reaction mixture was filtered and the precipitate was separated from the solution, washed with water and dried in air.

#### Synthesis of $\text{Mo}_8\text{O}_{26}(\text{C}_{10}\text{H}_{10}\text{N}_2)_2(\text{C}_5\text{H}_4\text{N})_2(\text{H}_2\text{O})_2$ (**2**)

Compound **2** was prepared similar to that of **1**, except that  $\text{Co}(\text{NO}_3)_2 \cdot 6\text{H}_2\text{O}$  (0.058 g) was used instead of  $\text{Cu}(\text{NO}_3)_2 \cdot 3\text{H}_2\text{O}$  and the reaction temperature was 150 °C.

#### Catalytic procedure

The oxidation of the dyes was carried out by air under room conditions. 1.33 g of either **1** or **2** was introduced into a fresh aqueous dye solution ( $C_0 = 0.3$  g/L, 100 ml) while stirring. The oxidant concentration depended on the solubility of oxygen under room conditions. At given intervals, a sample of the suspension (5 ml) was taken out by filtration. The solid was then filtered and washed with acetone and the filtrate was used for UV-Vis analysis to monitor the removal of the dyes. The color removal can be calculated as follows:

$$\text{Removal (\%)} = [(A_0 - A) / A_0] \times 100 \quad (\text{Eq. 1})$$

where  $A_0$  and  $A$  are the initial and final absorbance values of the dye, respectively.

#### X-ray single crystal data collection and refinement

X-ray intensity data for the **1** and **2** single crystals were collected using graphite monochromatic  $\text{MoK}\alpha$  radiation on a four-circle  $\kappa$  geometry KUMA KM-4 diffractometer with a two-dimensional area CCD detector. The  $\omega$ -scan technique with  $\Delta\omega = 1.0^\circ$  for each image was used for data collection. The 900 images for six different runs covering over 99 % of the Ewald sphere were performed. One image was used as a standard after every 50 images for monitoring of the crystals stability and the data collection. No correction on the relative intensity variations was necessary. Data collections were made using the CrysAlis CCD program [28]. Integration, scaling of the reflections, correction for Lorentz and polarisation effects and absorption corrections were performed using the CrysAlis Red program [28]. The structures were solved by the direct methods using SHELXS-97 and refined using SHELXL-97 program [29]. The hydrogen atoms joined to aromatic carbon atoms were introduced in their geometrical positions and refined as riding. All non-hydrogen atoms were refined anisotropically. The data were deposited in Cambridge crystallographic data center with deposition number CCDC 970132 (**1**) and 975177 (**2**). The detailed crystallographic data and structure refinement parameters for **1** and **2** are summarized in Table 1. Visualisations of the structures were made with the Diamond 3.0 program [30]. Selected geometrical parameters for **1** and **2** are listed in Table 2 and Table 3.

### Results and discussion

#### Structure of $(\text{NH}_4)_2\text{CuMo}_8\text{O}_{26}(\text{C}_{10}\text{H}_8\text{N}_2)_2$ (**1**)

Refinement of the crystal structure of **1** established that the occupation factor of  $\text{Cu}^{2+}$  cation is 0.5 and therefore it is statistically disordered. The asymmetric unit of **1** is composed of half  $\text{Cu}^{2+}$  cation, one neutral 4,4'-bpy molecule, one  $\text{NH}_4^+$  cation and half of an octamolybdate anion,  $[\text{Mo}_8\text{O}_{26}]^{4-}$  (Fig. 1a). Inversion related two asymmetric units are joined together forming centrosymmetric  $(\text{NH}_4)_2\text{CuMo}_8\text{O}_{26}(\text{C}_{10}\text{H}_8\text{N}_2)_2$  molecule (Fig. 1b) that contains the well known  $[\beta\text{-Mo}_8\text{O}_{26}]^{4-}$  cluster [31]. The  $[\beta\text{-Mo}_8\text{O}_{26}]^{4-}$  cluster consists of eight edge-shared  $\text{MoO}_6$  octahedra and four kinds of Mo—O bonds, with terminal ( $\text{O}_t$ ) and bridging  $\mu_2\text{-O}$ ,  $\mu_3\text{-O}$  and  $\mu_5\text{-O}$  oxygens. The shortest Mo—O distances are associated with the terminal oxygens ( $\text{O}_t$ ) whereas the longest distances are associated with the bridging  $\mu_5\text{-O}$  oxygens. The Mo—O distances increase with increasing of the number of the Mo cations bridged by O atoms (Table 2). All these Mo—O distances are in the range expected for the octahedrally coordinated Mo atoms of polyoxomolybdate clusters with small differences resulting from the distortion from the  $\text{O}_h$  geometry, and are in agreement with those described in the literature [32, 33]. The  $\text{Cu}^{2+}$  cation is coordinated to two nitrogen atoms from two translationally related 4,4'-bpy molecules to form  $[\text{CuN}_2]^{2+}$  unit. The coordination of  $[\text{CuN}_2]^{2+}$  is further completed by one terminal oxygen atom from  $[\beta\text{-Mo}_8\text{O}_{26}]^{4-}$  anion to adopt the T-shaped  $\{\text{CuN}_2\text{O}\}$  coordination geometry. The bond lengths around  $\text{Cu}^{2+}$  ions are Cu—N1, 1.720(8); Cu—N2<sup>i</sup>, 1.721(8) (symmetry code: (i) x, -1+y, z); Cu—O, 2.507(5) Å and the N1—Cu—N2 angle is 168.9(4)°. The relatively short Cu—N bonds can be explained by the disorder of the  $\text{Cu}^{2+}$  cation over two positions and by the relatively high anisotropic displacement parameters of the N and C atoms of the whole 4,4'-bpy molecule linked to Cu. The anisotropic thermal parameter  $U_{22}$  of N (and C) atoms along the Cu—N bonds is about four times greater than perpendicular to the Cu—N bonds ( $U_{11}$  and  $U_{33}$ ). Therefore the relatively high thermal parameters (especially  $U_{22}$ ) of the 4,4'-bpy molecules result from the half-occupied Cu atoms, and are responsible for the observed Cu—N bond length that is shorter than those reported for other POM-based structures [34-36].

The  $[\beta\text{-Mo}_8\text{O}_{26}]^{4-}$  anionic clusters can display a variety of coordination modes to form many interesting inorganic-organic hybrid materials [37, 38]. In **1**, the  $\text{MoO}_6$  octahedrons (shown as the yellow polyhedrons in Fig. 2) linked together to form  $[\beta\text{-Mo}_8\text{O}_{26}]^{4-}$  units that act as bidentate ligands through their terminal oxygen atoms. There are also weak interactions such as N—H $\cdots$ O hydrogen bonds between the  $\text{NH}_4^+$  cations and oxygen atoms of the  $[\beta\text{-Mo}_8\text{O}_{26}]^{4-}$  clusters forming 2D sheets parallel to the (001) plane. These 2D sheets are interconnected by C—H $\cdots$ O hydrogen bonds and together with the Cu—O interactions forming the 3D network (Fig. 3a and 3b).

#### Structure of $\text{Mo}_8\text{O}_{26}(\text{C}_{10}\text{H}_{10}\text{N}_2)_2(\text{C}_5\text{H}_4\text{N})_2(\text{H}_2\text{O})_2$ (**2**)

The molecular structure of **2** is illustrated in Fig. 4. The asymmetric unit of **2** consists of a quarter of  $\text{Mo}_8\text{O}_{26}(\text{C}_{10}\text{H}_{10}\text{N}_2)_2(\text{C}_5\text{H}_4\text{N})_2(\text{H}_2\text{O})_2$  molecule. Both protonated and non-protonated 4,4'-bpy units and water

molecule (O2W) are disordered. Two fold axis and inversion related four asymmetric  $[\text{Mo}_2\text{O}_{6.5}]^-$  parts are joined together forming the known  $[\beta\text{-Mo}_8\text{O}_{26}]^{4-}$  anionic cluster, which consists of eight edge-shared  $\text{MoO}_6$  distorted octahedra. Selected bond lengths and angles of **2** are listed in Table 3.

Figure 5 depicts a set of  $\text{C-H}\cdots\text{O}$  hydrogen bonding interactions between the disordered 4,4'-bpy ligands and oxygen atoms of the  $[\beta\text{-Mo}_8\text{O}_{26}]^{4-}$  anions that form the 3D network structure as illustrated in Fig. 6. The separated  $[\beta\text{-Mo}_8\text{O}_{26}]^{4-}$  anionic clusters are surrounded by organic protonated and non-protonated 4,4'-bpy units (both statistically disordered, occupation factor of 0.5) forming two-dimensional layers (Fig. 6a). There are multiple  $\text{O-H}\cdots\text{O}$  hydrogen bonding interactions between the water molecules (O1W) and the O atoms of the  $[\beta\text{-Mo}_8\text{O}_{26}]^{4-}$  anionic cluster with  $\text{O}\cdots\text{O}$  distance between 2.866(3) and 3.091(3) Å forming 1D polymeric motif along [001] direction, which is more distinctive feature of this structure (Fig. 6b).

In this work, we choose 4,4'-bpy as a rod-like ligand and copper as a secondary metal to synthesize **1** under solvothermal conditions. We tried to replace  $\text{Cu}(\text{NO}_3)_2\cdot 3\text{H}_2\text{O}$  with  $\text{Ni}(\text{NO}_3)_2\cdot 6\text{H}_2\text{O}$  or  $\text{Zn}(\text{NO}_3)_2\cdot 6\text{H}_2\text{O}$ , but no suitable crystals for single-crystal X-ray diffraction were formed. When  $\text{Co}(\text{NO}_3)_2\cdot 6\text{H}_2\text{O}$  was used as the salt of secondary transition metal the novel hybrid compound **2** was obtained, although Co (II) ions did not appear in the structure. In POM-based inorganic-organic compounds, copper ions are the most often encountered secondary transition metal ions probably owing to long Cu—O distance that avoid the steric hindrance of POM anion and allow the connection between the bulky POM and the copper complex [39].

#### Thermogravimetric analyses

Thermal stability of compounds **1** and **2** was examined by thermogravimetric analysis (TGA). As shown in Fig. 7, for compound **1**, ammonium ions are released from 100 °C to about 225 °C (observed 2%, calculated 2.3 %). The organic ligands begin to decompose at 225 °C. The final residue can be attributed to molybdenum copper mixed-oxide. The TG curve of compound **2** shows the first weight loss from 100 °C to about 225 °C corresponding to two water molecules (observed 2.6 %, calculated 2.13 %). The decomposition of the organic molecules occurs above 225 °C. The final residue might be related to molybdenum oxide compound.

#### Nanostructure of **1**

Compound **2** comprises discrete entities that are connected via hydrogen bonds constructing a 3D network, while compound **1** consists of 1D coordinating chains. In order to study whether the size of the crystals may affect the catalytic properties, the top-down approach has been utilized to prepare **1** in nano-scale under ultrasound irradiation. The SEM image of the nanostructured **1** shown in Fig. 8 indicates spherical morphology. The PXRD patterns (Fig. 9) and the FT-IR spectra (Fig. 10) of the nanostructured polymer are identical to the corresponding bulk polymer pattern indicating no structural deformation upon ultra-sonication.

As shown in Fig. 10, the FT-IR spectra of the crystals exhibited the bands attributed to Mo-O and Mo-O-Mo vibrations in the range of 680-943  $\text{cm}^{-1}$  for **1** and 672-941  $\text{cm}^{-1}$  for **2** that are almost identical to those of the reported octamolybdate compounds. In addition, the peaks located at 1410-1613  $\text{cm}^{-1}$  can be assigned to the characteristic peaks of the 4,4'-bpy ligand [32, 38].

#### Catalytic wet air oxidation

To evaluate the catalytic activity of the prepared octamolybdate-based compounds, the decolorization of some dyes (Fig. S1) such as Bismarck brown (BB), Azure II, Direct blue 71 (DB 71), Methyl violet (MV) and Methylene blue (MB) was studied under mild conditions. The color removal efficiency of the dyes after 2 h (Fig. 11) was calculated from Eq. 1 and their corresponding UV-Vis spectra in the presence of the catalysts are shown in Fig. S2-S6. It is evident that the prepared compounds can act as active catalysts in the CWAO process of the dyes using air as oxidant. Bismarck brown as a representative dye was selected for the early exploration of the CWAO process. Fig. 12 depicts the UV-Vis spectra for the degradation of Bismarck brown solution within different reaction time while Fig. 13 presents the change of its color removal efficiency calculated from Eq. 1 at  $\lambda_{\text{max}} = 457$  nm as a function of time. A noticeable point when comparing the results in Fig. 13 is that the catalytic activity of compound **1** and **2** is comparable after 60 min. It seems that the catalytic activity of **1** mainly originates from octamolybdate clusters rather than Cu (II) ions. To the best of our knowledge, the catalytic activity of octamolybdate-based compounds in CWAO of dyes has not been explored. However, these compounds have been applied as photocatalysts for dye degradation [40-43]. In order to get a better insight into the catalytic activity of octamolybdate cluster in the CWAO process, we have prepared tetrabutylammonium octamolybdate,  $[(\text{n-C}_4\text{H}_9)_4\text{N}]_4[\text{Mo}_8\text{O}_{26}]$  according to the previously reported method [44] and utilized it for the CWAO of Bismarck brown under the same reaction conditions. The FT-IR spectrum of the prepared  $[(\text{n-C}_4\text{H}_9)_4\text{N}]_4[\text{Mo}_8\text{O}_{26}]$  exhibits the peaks for octamolybdate cluster (Fig. S7) [38]. The UV-Vis spectrum of Bismarck brown after decolorization in the presence of  $[(\text{n-C}_4\text{H}_9)_4\text{N}]_4[\text{Mo}_8\text{O}_{26}]$  for 2 h is shown in Fig. S8. The results show that Bismarck brown solution efficiently decolorized in the presence of tetrabutylammonium octamolybdate compound.

From Fig. 13, it can be observed that the nanocrystals of **1** exhibit higher activity within short period of time compared to the corresponding bulk catalyst. In order to clear up the catalytic effect of the prepared compounds, we have included the results of the degradation process without the presence of the catalysts and only with air under the same conditions. The result shows that the color removal of the dye solution is negligible confirming the limited oxidation ability of oxygen in the absence of the catalyst under room conditions.

The FT-IR spectra of Bismarck brown before and after the catalytic reaction are presented in Fig. 14. The FT-IR spectrum of Bismarck brown exhibits aromatic ring C-H stretching vibration peaks at 3156  $\text{cm}^{-1}$  and aromatic ring C-H bending vibrations at 875 and 709  $\text{cm}^{-1}$ . The peaks appeared in region 1520-1627  $\text{cm}^{-1}$  are related to the aromatic ring C=C stretching vibration peaks. The peak located at 1242  $\text{cm}^{-1}$  is due to the C-N stretching vibration of Bismarck brown. After the treatment of the dye for about 30 min, these peaks decrease in intensity to disappear that shows the destruction of Bismarck brown structure. Also the ion chromatography (IC) analysis of the dye solution after decolorization showed that the Bismarck brown mineralized into inorganic species such as  $\text{NO}_3^-$ ,  $\text{NH}_4^+$  and  $\text{Cl}^-$  suggesting the catalytic process of the color removal (Fig. S9).

The recyclability of the catalysts was studied in the CWAO reaction of Bismarck brown for three times (Fig. 15). After each run, the mixture was filtered and the catalysts were collected and completely washed with acetone and water prior to use for the next cycle. The obtained results show that the recovered catalysts maintained similar catalytic activities after three recycles. The atomic absorption spectroscopy of the catalysts shows no considerable loss of the molybdenum content (Table 4) after the reactions. Moreover, the PXRD patterns (Fig. 9) and the FT-IR spectra (Fig. 10) of the recycled catalysts show no significant change in the structure of the catalysts suggesting that the catalysts are stable under the reaction conditions.

## Conclusion

Two new octamolybdate-based hybrid materials **1** and **2** have been solvothermally synthesized and structurally characterized. Compound **1** has also been sonochemically prepared in nanoscale with the preservation of crystal structure. The catalytic activity of the compounds has been studied in the degradation of some dyes under mild conditions. The obtained results show that the prepared compounds are efficient heterogeneous catalysts in terms of both activity and stability.

## Acknowledgment

The authors would appreciate the financial support from University of Tehran.

## References

- 1 J. Fu and G. Z. Kyzas, *Chin. J. Catal.*, 2004, **35**, 1.
- 2 M. D. Chengalroyen and E. R. Dabbs, *World J. Microbiol. Biotechnol.*, 2013, **29**, 389.
- 3 A. El-Ghenymy, F. Centellas, J. A. Garrido, R. M. Rodríguez, I. Sirés, P. L. Cabot and E. Brillas, *Electrochem. Acta*, 2014, **130**, 568.
- 4 S.-M. Lam, J.-C. Sin, A. Z. Abdullah, A. R. Mohamed, *Desalin. Water Treat.*, 2012, **41**, 131.
- 5 L. Gomathi, K. S. A. Raju, S. G. Kumar, K. E. Rajashekhar, *J. Taiwan Inst. Chem. E.*, 2011, **42**, 341.
- 6 M. A. Tariq, M. Faisal and M. Muneer, *J. Hazard. Mater.*, 2005, **127**, 172.
- 7 M. A. Rauf, S. S. Ashraf, *Chem. Eng. J.*, 2012, **209**, 520.
- 8 S. Deng, H. Xu, X. Jiang and J. Yin, *Macromolecules*, 2013, **46**, 2399.
- 9 K.-H. Kim and S.-K. Ihm, *J. Hazard. Mater.*, 2011, **186**, 16.
- 10 M. Yuan, S. Wang, X. Wang, L. Zhao and T. Hao, *Appl. Surf. Sci.*, 2011, **257**, 7913.
- 11 J. Huang, X. Wang, S. Li and Y. Wang, *Appl. Surf. Sci.*, 2010, **257**, 116.
- 12 H. Ma, Q. Zhuo and B. Wang, *Environ. Sci. Technol.*, 2007, **41**, 7491.
- 13 Y. Zhang, D. Li, Y. Chen, X. Wang and S. Wang, *Appl. Catal. B: Environ.*, 2009, **86**, 182.
- 14 A. Dolbecq, P. Mialane, B. Keita and L. Nadjo, *J. Mater. Chem.*, 2012, **22**, 24509.
- 15 Q. Wu, X. Hao, X. Feng, Y. Wang, Y. li, E. Wang, X. Zhu and X. Pan, *Inorg. Chem. Commun.*, 2012, **22**, 137.
- 16 I. Arslan-Alaton and J. L. Ferry, *Dyes Pigments*, 2002, **54**, 25.
- 17 F. Changgen, Z. Xiaoxi and L. Xia, *J. Rare Earth*, 2009, **27**, 717.
- 18 W. Yajun, L. Kecheng and F. Changgen, *J. Rare Earth*, 2013, **31**, 360.
- 19 J. Yan, X. Zhao, J. Huang, K. Gong, Z. Han and X. Zhai, *J. Solid State Chem.*, 2014, **211**, 200.
- 20 T. Li, S. Gao, F. Li and R. Cao, *J. Colloid Interface Sci.*, 2009, **338**, 500.
- 21 Z. Sun, W. Wang, S. Wang, C. Wang, D. Lu, Y. Gao, W. Hao and P. Yan, *J. Inorg. Organomet. Polym.*, 2014, **24**, 706.
- 22 M. Najafi, A. Abbasi, M. Masteri-Farahani and V. H. Rodrigues, *Inorg. Chem. Commun.*, 2014, **46**, 251.
- 23 F. Novio, J. Simmchen, N. Vázquez-Mera, L. Amorín-Ferré and D. Ruiz-Molina, *Coord. Chem. Rev.*, 2013, **257**, 2839.
- 24 S. Hojaghani, M. H. Sadr and A. Morsali, *Dyes Pigments*, 2014, **104**, 204.
- 25 M. J. Soltanian Fard, N. Ghanbari and F. Rastaghi, *Inorg. Chim. Acta*, 2013, **396**, 149.
- 26 M. J. Soltanian Fard and F. Rastaghi, *J. Mol. Struct.*, 2014, **1063**, 289.
- 27 B. Zhou, F.-C. Xu, J. Yang, J. Yao and Y.-H. Xiao, *Mater. Lett.*, 2013, **107**, 206.
- 28 CrysAlis CCD and CrysAlis RED program, Ver. 171.32.6, Oxford Diffraction Poland, Wrocław, Poland, 2006.
- 29 G. M. Sheldrick, *Acta Cryst.* 2008, **A64**, 112.
- 30 K. Brandenburg, H. Putz, DIAMOND, Version 3.0, Crystal Impact GbR, Bonn, Germany, 2006.
- 31 C. J. G. Garcia, E. Coronado, S. Triki, L. Ouahan, P. Delhaes, *Adv. Mater.*, 1993, **5**, 283.
- 32 J. Luo, M. Hong, R. Wang, Q. Shi, R. Cao, J. Weng, R. Sun and H. Zhang, *Inorg. Chem. Commun.*, 2003, **6**, 702.
- 33 H.-H. Yu, X.-B. Cui, J. Lu, Y.-H. Sun, W.-J. Duan, J.-W. Cui, Z.-H. Yi, J.-Q. Xu and T.-G. Wang, *J. Mol. Struct.*, 2008, **879**, 156.
- 34 H. Jin, X. Wang, Y. Qi and E. Wang, *Inorg. Chim. Acta*, 2007, **360**, 3347.
- 35 H. Fu, W. Chen, E. Wang, J. Liu and S. Cheng, *Inorg. Chim. Acta*, 2009, **362**, 1412.
- 36 G. Li, C. Salim and H. Hinode, *Solid State Sci.*, 2008, **10**, 121.
- 37 H.-Y. Liu, H. Wu, J.-F. Ma, Y.-Y. Liu, J. Yang and J.-C. Ma, *Dalton Trans.*, 2011, **40**, 602.
- 38 W.-Q. Kan, J. Yang, Y.-Y. Liu and J.-F. Ma, *Dalton Trans.*, 2012, **41**, 11062.
- 39 A. Dolbecq, E. Dumas, C. R. Mayer and P. Mialane, *Chem. Rev.*, 2010, **110**, 6009.

- 40 W. Wang, J. Yang, W.-Q. Kan and J.-F. Ma, *Cryst. Eng. Comm.*, 2013, **15**, 5844.  
41 X. Wang, N. Han, H. Lin, A. Tian, G. Liu and J. Zhang, *Dalton Trans.*, 2014, **43**, 2052.  
42 H.-Y. Liu, L. Bo, J. Yang, Y.-Y. Liu, J.-F. Ma and H. Wu, *Dalton Trans.*, 2011, **40**, 9782.  
43 W. Sun, C. Zhang, H. Ma, H. Pang and S. Li, *Dalton Trans.*, 2014, **43**, 16322.  
44 W. G. Klemperer, *Inorganic syntheses*, John Wiley and Sons, 1990, Vol. 27, Ch. 3, P. 78.

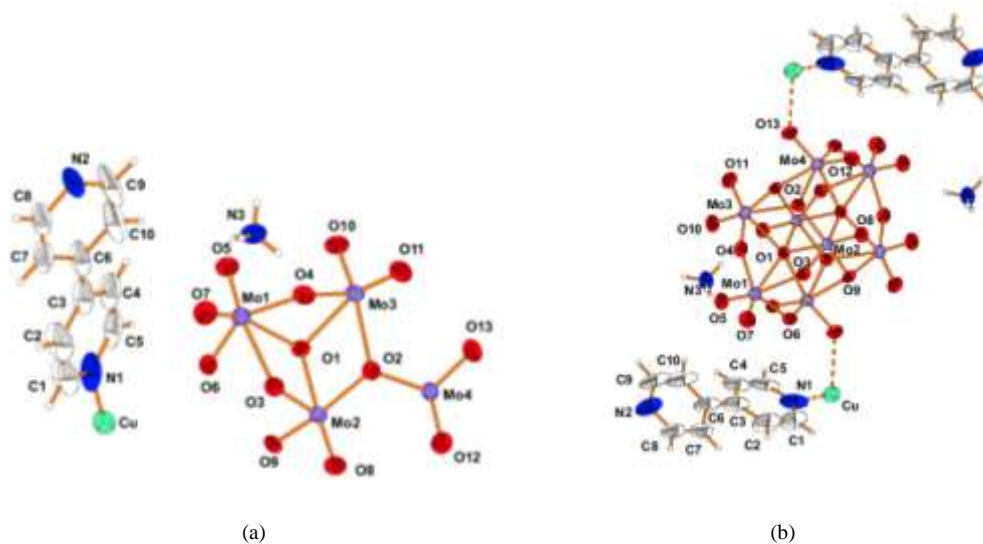


**Fig. 1.** (a) View of the asymmetric unit and (b) the centrosymmetric molecule of **1**. The Cu cation occupied statistically two positions. Thermal ellipsoids were scaled to 50 % probability level. H atoms with arbitrary radii.

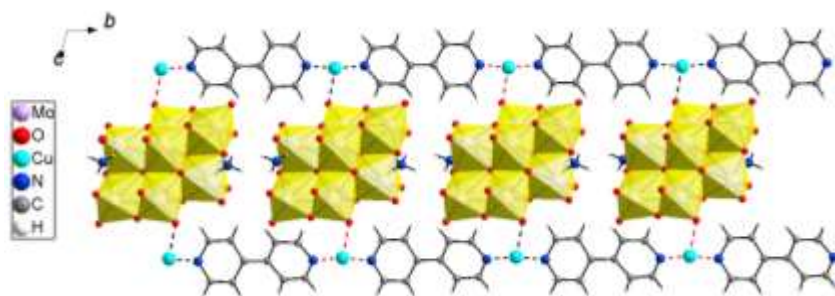
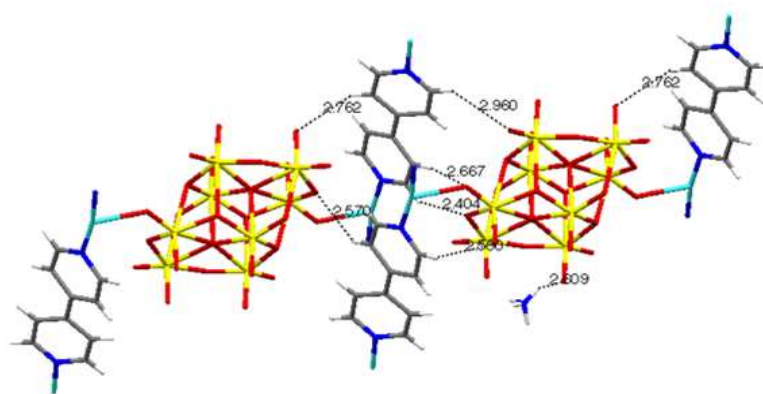
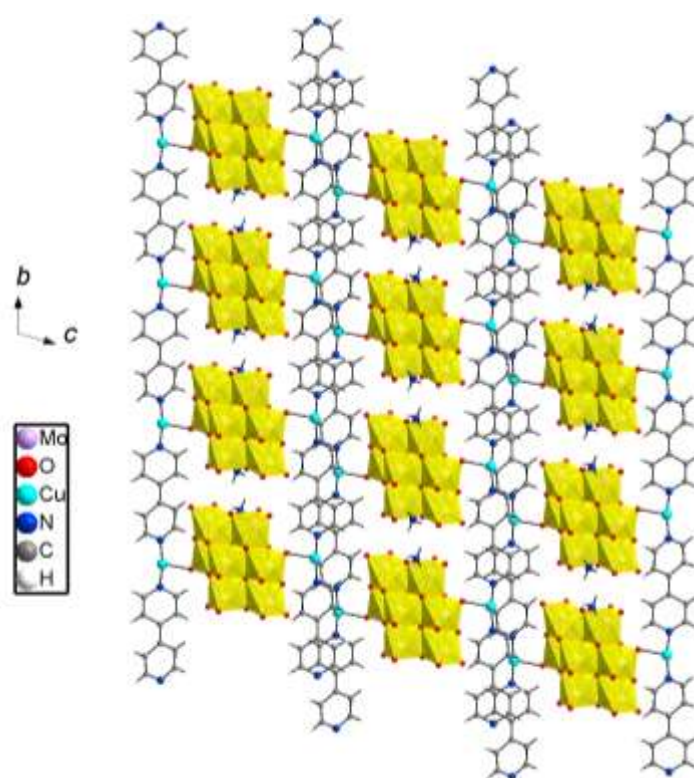


**Fig. 2.** View of 1D coordinating chain in **1**. Yellow polyhedrons consist of  $\text{MoO}_6$  octahedrons linked together to form octamolybdate clusters. The occupation factor of Cu cation is 0.5.



(a)



(b)

**Fig. 3.** (a) Non-covalent interactions and (b) view along  $a$ -axis of the 3D network for **1**. (The yellow polyhedrons represent  $\text{MoO}_6$  octahedrons that are connected to form octamolybdate clusters.)

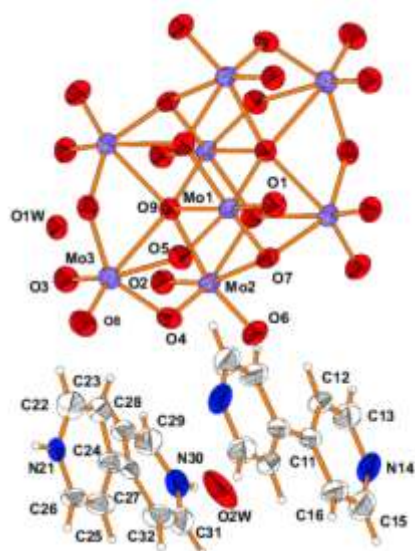


**Fig. 4.** View of the molecular structure of **2**. The water O2W, protonated and non-protonated 4,4'-bpy have occupation factor of 0.5. Thermal ellipsoids for Mo and O atoms of  $\text{Mo}_8\text{O}_{26}^{4-}$  and O1W were scaled to 50 % probability level, whereas for both disordered 4,4'-bpy units and water O2W were scaled to 30% probability level. H atoms with arbitrary radii.

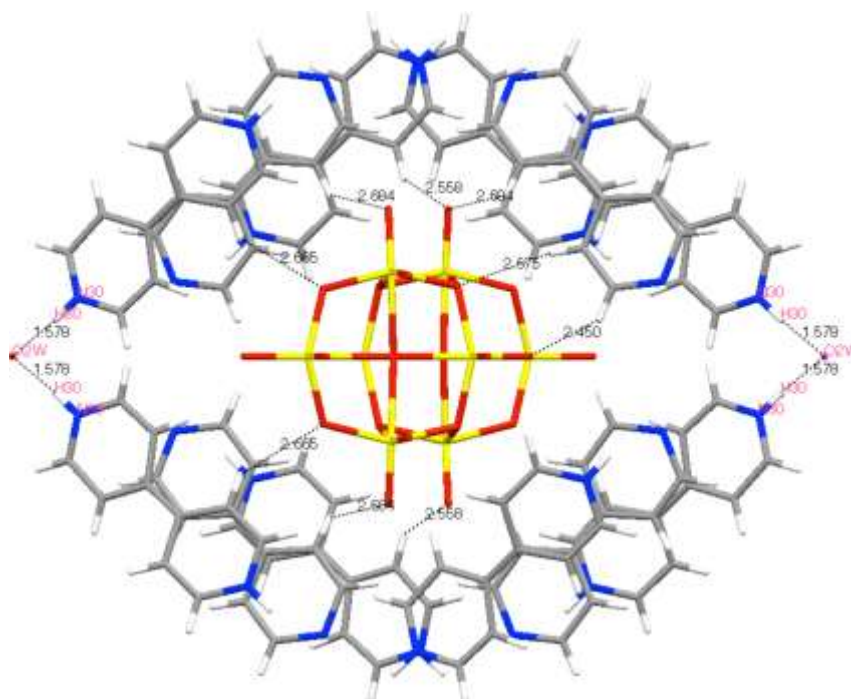


**Fig. 5.** Hydrogen-bonding interactions for **2**. The water O2W, protonated and non-protonated 4,4'-bpy have occupation factor of 0.5.

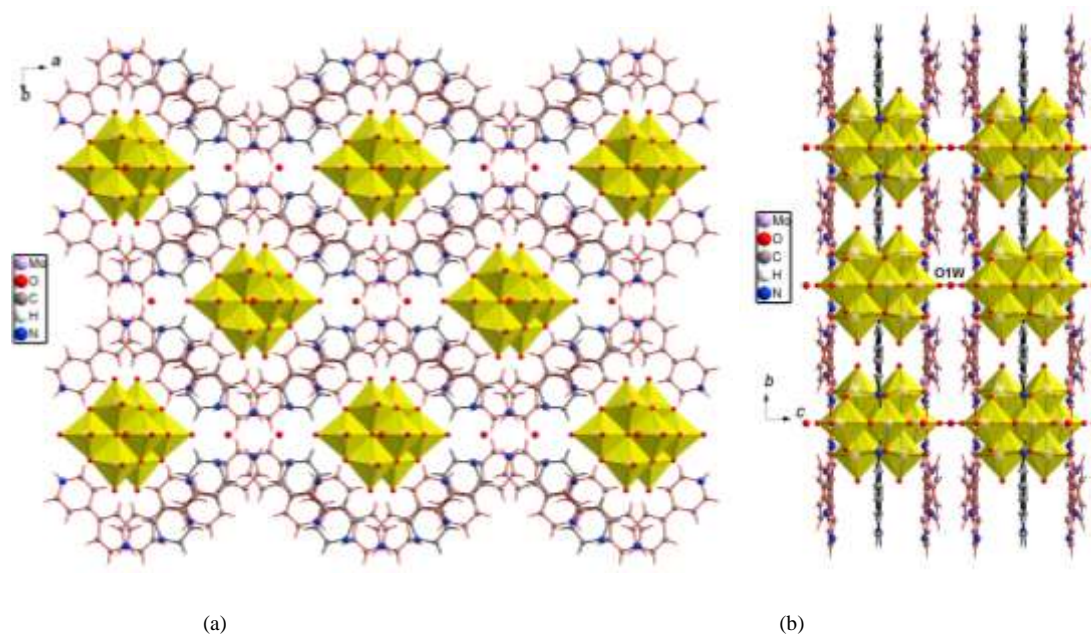


**Fig. 6.** View along *c*-axis (a) and *a*-axis (b) of the packing diagram of **2**. The disordered protonated and non-protonated 4,4'-bpy units are marked in orange and black, respectively.

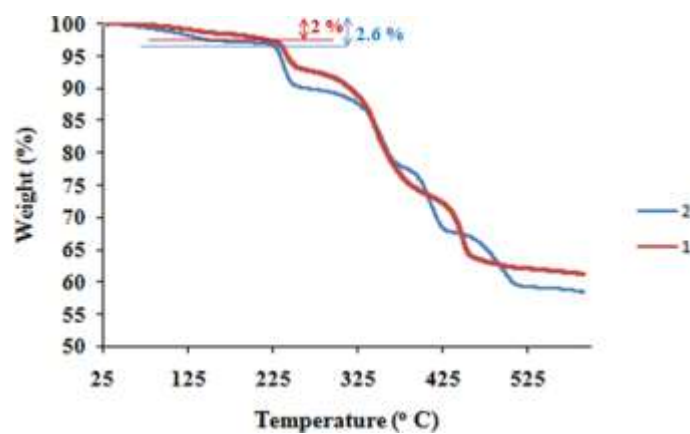


**Fig. 7.** TG curves for compound **1** and **2**.

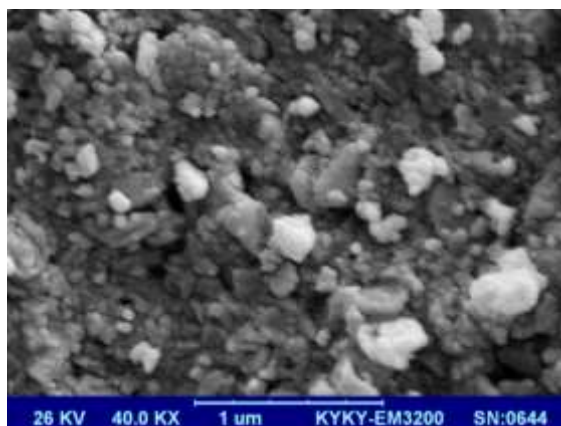


Fig. 8. SEM image of nanostructured 1.

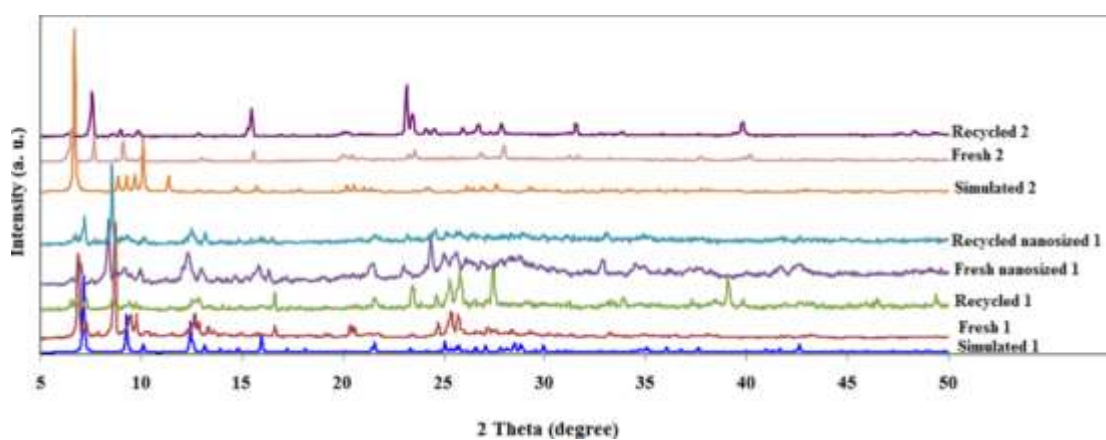


Fig. 9. PXRD patterns of  $(\text{NH}_4)_2\text{CuMo}_8\text{O}_{26}(\text{C}_{10}\text{H}_8\text{N}_2)_2$  (1) and  $\text{Mo}_8\text{O}_{26}(\text{C}_{10}\text{H}_{10}\text{N}_2)_2(\text{C}_{10}\text{H}_8\text{N}_2)_2(\text{H}_2\text{O})$  (2).

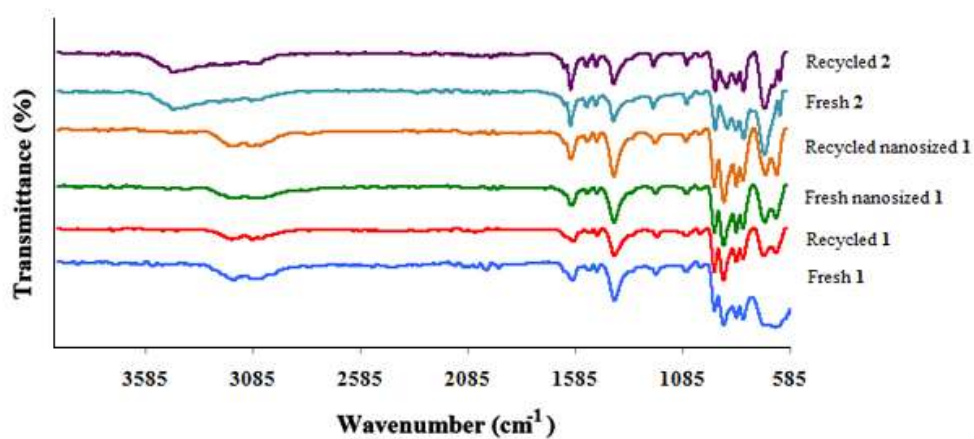


Fig. 10. FT-IR spectra of  $(\text{NH}_4)_2\text{CuMo}_8\text{O}_{26}(\text{C}_{10}\text{H}_8\text{N}_2)_2$  (1) and  $\text{Mo}_8\text{O}_{26}(\text{C}_{10}\text{H}_{10}\text{N}_2)_2(\text{C}_{10}\text{H}_8\text{N}_2)_2(\text{H}_2\text{O})$  (2)

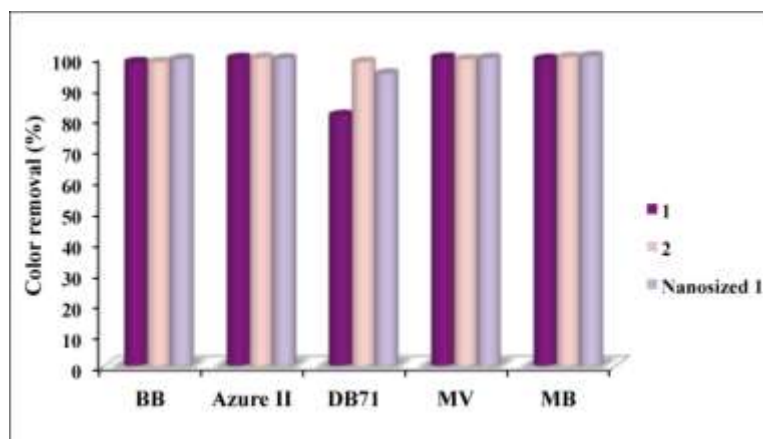


Fig. 11. Color removal efficiency of some dyes in the presence of the prepared catalysts after 2 h. (BB = Bismarck brown, DB 71 = Direct blue 71, MV = Methyl violet and MB = Methylene blue).

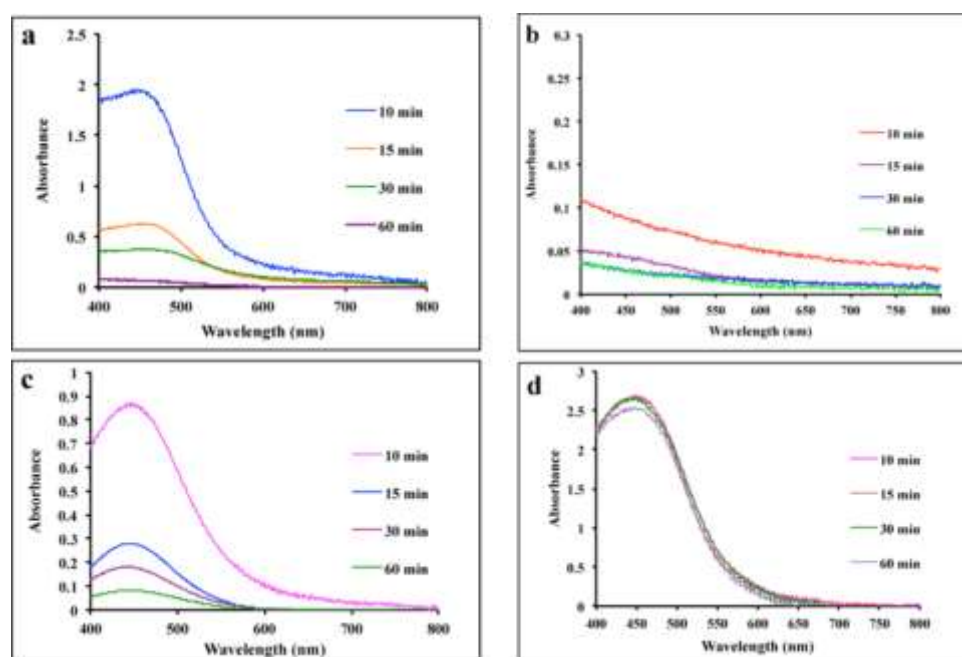


Fig. 12. Absorption spectra of the Bismarck brown solution during the decomposition reaction in the presence of (a) compound 1 (b) nanosized 1 (c) compound 2 and (d) in the absence of the catalysts

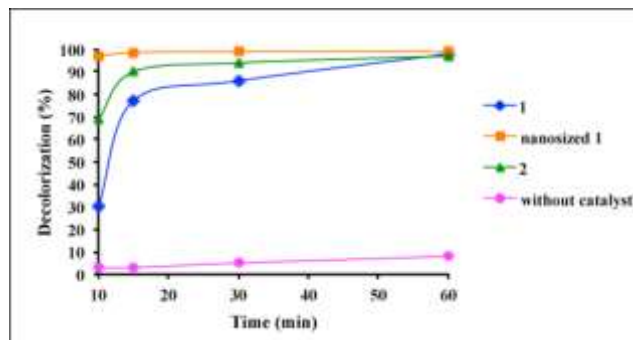


Fig. 13. Decolorization efficiency of Bismarck brown in the presence of the prepared catalysts.

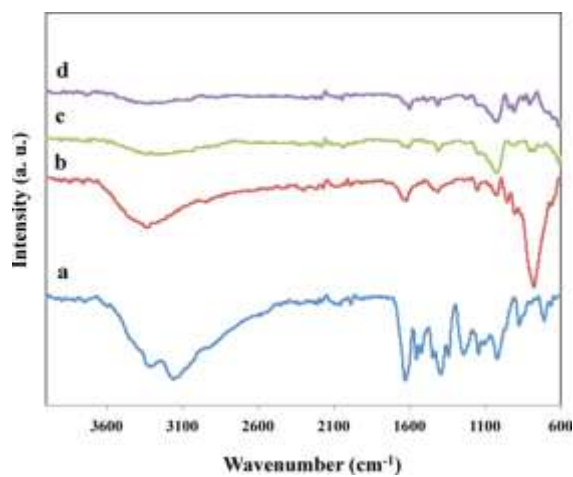


Fig. 14. Changes of the FT-IR spectra of Bismarck brown (a) before treatment, and after the reaction in the presence of (b) compound 1, (c) nanosized 1 and (d) compound 2 after 30 min treatment.

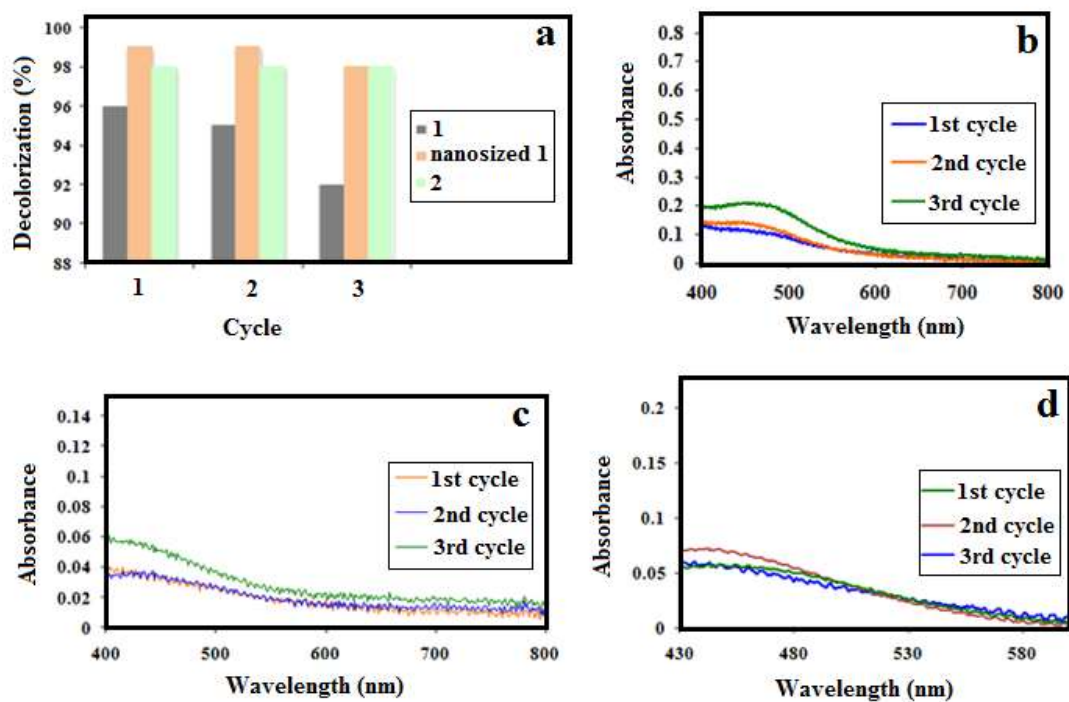


Fig. 15. (a) Decolorization efficiency of Bismarck brown in the presence of the recycled catalysts and absorption spectra of the dye solution during the degradation reaction in the presence of (b) compound 1 (c) nanosized 1 (d) compound 2.

**Table 1.** Crystal and structure refinement data for compounds **1** and **2**.

Compound	<b>1</b>	<b>2</b>
Empirical formula	C <sub>20</sub> H <sub>24</sub> CuMo <sub>8</sub> N <sub>6</sub> O <sub>26</sub>	C <sub>30</sub> H <sub>30</sub> Mo <sub>8</sub> N <sub>6</sub> O <sub>28</sub>
Molecular weight	1595.51	1690.10
Crystal system	triclinic	monoclinic
Space group	P-1	C2/m
Temperature (K)	295(2)	295(2)
Wavelength (Å)	0.71073	0.71073
<i>a</i> (Å)	7.7964(5)	18.8599(8)
<i>b</i> (Å)	10.4432(5)	19.0464(7)
<i>c</i> (Å)	13.0463(10)	10.2919(4)
<i>α</i> (°)	100.635(5)	90.00
<i>β</i> (°)	100.924(6)	104.635(4)
<i>γ</i> (°)	108.981(5)	90.00
Cell volume (Å <sup>3</sup> )	950.96(11)	3577.0(2)
<i>Z</i>	1	2
Crystal size (mm)	0.18×0.18×0.08	0.21×0.18×0.08
$\rho$ (g cm <sup>-3</sup> )	2.786	1.567
$\mu$ (mm <sup>-1</sup> )	3.195	1.419
Absorption correction	numerical	numerical
<i>T</i> <sub>min</sub> / <i>T</i> <sub>max</sub>	0.6078 / 0.7167	0.7633 / 0.9078
Total reflections	11049	21141
Unique reflections	4702	4795
Observed reflections [ <i>F</i> <sup>2</sup> > 2σ( <i>F</i> <sup>2</sup> )]	3432	3240
<i>R</i> <sub>int</sub>	0.0241	0.0247
Data/restraints/parameters	3432/4/292	3240/0/260
Goodness-of-fit (GOF) on <i>F</i> <sup>2</sup>	1.001	1.003
<i>R</i> [ <i>F</i> <sup>2</sup> > 2σ( <i>F</i> <sup>2</sup> )] ( <i>R</i> <sub>1</sub> , <i>wR</i> <sub>2</sub> ) <sup>a)</sup>	0.0350, 0.0675	0.0334, 0.0660
<i>R</i> (all data) ( <i>R</i> <sub>1</sub> , <i>wR</i> <sub>2</sub> )	0.0593, 0.0784	0.0658, 0.0788
$\Delta\rho_{\max}$ , $\Delta\rho_{\min}$ (e Å <sup>-3</sup> )	+ 0.748, -0.751	+0.768, -0.402

<sup>a)</sup>  $wR_2 = \{\sum [w(F_o^2 - F_c^2)^2] / \sum wF_o^4\}^{1/2}$ ;  $w^{-1} = 1/[\sigma^2(F_o^2) + (aP)^2 + (bP)]$  where *a* and *b* are 0.0304 and 3.0681 for **1** and 0.038 and 3.3806

for **2**, and  $P = (F_o^2 + 2F_c^2)/3$ .

**Table 2.** Selected bond lengths (Å) and angles (°) for compound **1**.

Bond lengths (Å):					
<b>O<sub>t</sub></b> - terminal					
Mo1—O5	1.721(4)	Mo1—O7	1.699(4)	Mo3—O10	1.713(4)
Mo3—O11	1.699(4)	Mo4—O12	1.699(3)	Mo4—O13	1.703(4)
<b>μ<sub>2</sub>-O</b>					
Mo1—O3	2.276(3)	Mo2—O3	1.749(3)	Mo1—O4	1.936(3)
Mo3—O4	1.911(3)	Mo1—O6	1.904(3)	Mo4 <sup><i>i</i></sup> —O6	1.916(3)
<b>μ<sub>3</sub>-O</b>					
Mo2—O2	1.949(3)	Mo3—O2	2.354(3)	Mo4—O2	1.999(3)
Mo2—O9	1.966(3)	Mo3 <sup><i>i</i></sup> —O9	1.985(3)	Mo4 <sup><i>i</i></sup> —O9	2.350(3)
<b>μ<sub>5</sub>-O</b>					
Mo1—O1	2.477(3)	Mo2—O1	2.366(3)	Mo3—O1	2.338(3)
Mo2 <sup><i>i</i></sup> —O1	2.150(3)	Mo4 <sup><i>i</i></sup> —O1	2.316(3)		
Bond angles (°):					
O3—Mo1—O1	69.84(10)	O4—Mo1—O1	73.91(12)		
O5—Mo1—O1	93.86(15)	O6—Mo1—O3	77.49(13)		
O7—Mo1—O3	90.62(15)	O5—Mo1—O4	97.31(16)		
O5—Mo1—O6	98.82(16)	O7—Mo1—O5	105.68(19)		
O7—Mo1—O6	101.66(17)	O2—Mo2—O1	77.87(12)		
O3—Mo2—O1	81.48(13)	O9—Mo2—O1	78.12(12)		
O8—Mo2—O2	101.86(15)	O8—Mo2—O9	99.62(15)		
O3—Mo2—O9	96.48(14)	O8—Mo2—O3	106.04(15)		
O3—Mo2—O9	96.48(14)	O1—Mo3—O2	71.20(11)		
O4—Mo3—O1	77.77(12)	O11—Mo3—O2	88.13(15)		
O11—Mo3—O4	100.20(16)	O10—Mo3—O4	100.64(16)		
O11—Mo3—O10	105.16(19)	O12—Mo4—O2	97.64(15)		
O13—Mo4—O2	102.44(15)	O12—Mo4—O13	105.55(18)		

Symmetry code: (*i*) 0.5-x, 0.5-y, -z.

**Table 3.** Selected bond lengths (Å) and angles (°) for compound **2**.

Bond length (Å)		Bond angles (°)	
Mo1—O1	1.689 (3)	O1—Mo1—O5	104.68(14)
Mo1—O5	1.762 (3)	O5—Mo1—O7	96.04(7)
Mo1—O7	1.958 (2)	O1—Mo1—O7	101.73(6)
Mo1—O9	2.398 (3)	O5—Mo1—O9	80.25(11)
Mo1—O9 <sup>i</sup>	2.140 (3)	O2—Mo2—O6	104.53(11)
Mo2—O2	1.709 (2)	O2—Mo2—O4	101.89(10)
Mo2—O4	1.895 (2)	O4—Mo2—O6	102.17(11)
Mo2—O6	1.701(2)	O4—Mo2—O7	82.57(8)
Mo2—O7	2.366 (2)	O3—Mo3—O4	97.84(7)
Mo2—O7 <sup>i</sup>	2.007(2)	O3—Mo3—O8	106.27(17)
Mo2—O9	2.324 (5)	O3—Mo3—O9	92.64(13)
Mo3—O3	1.710 (3)	Mo1—O5—Mo3	118.46(14)
Mo3—O4	1.915 (2)	Mo1—O7—Mo2	110.35 (9)
Mo3—O5	2.266 (3)	Mo1—O9—Mo2	97.75(6)
Mo3—O8	1.715 (3)	Mo1—O9—Mo3	91.07(9)
Mo3—O9	2.464 (3)	Mo2—O4—Mo3	117.67(11)

Symmetry code: (i)  $-x, y, -z$ ;**Table 4.** Metal content of the catalysts.

Catalyst	Mo content in fresh catalyst (%)	Mo content in recovered catalyst (%)	Cu content in fresh catalyst (%)	Cu content in recovered catalyst (%)
<b>1</b>	38.7	38.4	3.9	3.5
Nanosized <b>1</b>	43.9	42.6	4.2	4.2
<b>2</b>	39.3	39.2	-	-